







# Distribution Matching for Dimming Control in Visible-Light Region-of-Interest Signaling

Phuc Duc Nguyen , *Member, IEEE*, Yoshifumi Shiraki , *Member, IEEE*, Kenji Ishikawa ,  
Jun Muramatsu , *Senior Member, IEEE*, Noboru Harada , *Senior Member, IEEE*,  
and Takehiro Moriya , *Life Fellow, IEEE*

**Abstract**—We propose a two-level dimmer based on binary distribution matching where a low-rate signal controls the output probability distribution of a high-rate bit sequence, which can be used in region-of-interest (RoI) signaling applications. To reduce the rate loss of the dimmer, we propose the extended multiset-partition distribution matching (EMPDM) algorithm with a novel binary-tree-structure implementation. In addition, we introduce 4p-EMPDM, a compact version of EMPDM, which has a typical composition (TC) and four leading composition pairs (CPs). The codebook of 4p-EMPDM includes only run-length-aware code-words, which reduces the maximum run-length of the transmitted bit sequence by 4.27 times. Hence, it guarantees flicker mitigation for visible-light RoI signaling systems at 6 kHz without using any run-length limited code (non-RLL). Using experimental data collected from the low-rate RoI signaling prototype, we introduced a threshold range where both intensity and area information of the received training symbols can be exploited to optimize the shaping ratios of the 4p-EMPDM dimmer. Because of the non-RLL feature, the proposed system can support soft-decision forward-error-correction (FEC) decoding to improve reliability. Our system outperforms related systems based on hybrid modulation schemes in terms of spectral efficiency, bit rate, and minimum required optical clock rate.

**Index Terms**—Probabilistic shaping, distribution matching, dimming control, region-of-interest signaling, visible light communication.

## I. INTRODUCTION

VISIBLE-LIGHT region-of-interest (RoI) signaling has been introduced for vehicular optical camera communication (OCC) systems by IEEE 802.15.7 m group (TG7m) [1]. This technique enables the OCC systems to transmit simultaneously low-rate and high-rate data streams. Where the low-rate stream is used for RoI identification, the high-rate stream, on the other hand, is used for high-speed data communication on the selected RoI. Hybrid modulation schemes such as twinkle

variable pulse position modulation (VPPM) and hybrid spatial phase-shift keying (HS-PSK) are popular in modulating the low-rate and high-rate streams. Specifically, the high-rate stream is modulated by twinkle VPPM or dimming spatial-8 phase-shift keying (DS8-PSK) [2], whereas, the low-rate stream is modulated by undersampled frequency-shift on-off keying (UF-SOOK), undersampled phase-shift on-off keying (UPSOOK), or spatial-2 phase-shift keying (S2-PSK) [3]. Both streams sent from a RoI are decoded by a dual-camera receiver, where the high-speed (HS) camera demodulates the high-rate stream, and the low-speed (LS) camera demodulates the low-rate stream. As a result, the computational load of the HS-camera-based receiver is reduced.

Dimming control is one of the critical problems in OCC and visible light communication (VLC) systems. In conventional approaches, dimming control uses compensation symbol insertion and puncturing, which adds numerous redundant bits to the frame, resulting in a degraded achievable rate [4]. The dimming level can be managed by adjusting the OFF (0's) or ON (1's) ratio in the bit stream from 0% to 100%. The dimming control in HS-PSK and twinkle VPPM changes the duty cycle of groups of high-rate pulses. Hence, it is challenging to demodulate DS8-PSK and twinkle VPPM signals because each pulse must be synchronized, sampled, and decoded at a critical timing [5]. In addition, in conventional VLC systems, long runs of 1's and 0's, which cause flicker and clock and data recovery (CDR) issues, should be avoided. Hence, run-length-limited (RLL) codes keep a direct current (DC) balance with equal numbers of 1's and 0's in every symbol. There is a trade-off between rate loss and ease of implementation in RLL codes such as Manchester, 4B6B, and 8B10B [6]. Additionally, only hard-decision (HD) forward error correction (FEC) decoders are supported in joint FEC-RLL-based systems because most RLL decoders produce hard output information, which degrades error-correction performance. A soft-input soft-output (SISO) RLL decoder introduced by Kim et al. [7] generates soft output information for soft-decision (SD) FEC decoding algorithms to improve the system reliability. However, the decoding algorithm of the SISO RLL code is complex and infeasible to incorporate in VLC receivers.

Layered probabilistic shaping (LPS) is a probabilistically shaped coded modulation scheme that employs a distribution matcher (DM) followed by a systematic channel encoder at the transmitter, and a systematic channel decoder followed by an

Manuscript received 2 November 2022; revised 14 December 2022; accepted 27 December 2022. Date of publication 13 January 2023; date of current version 20 January 2023. (Corresponding author: Phuc Duc Nguyen.)

Phuc Duc Nguyen, Yoshifumi Shiraki, Kenji Ishikawa, and Noboru Harada are with the NTT Communication Science Laboratories, Nippon Telegraph and Telephone Corporation, Atsugi, Kanagawa 243-0198, Japan (e-mail: phucd.nguyen@ntt.com; yoshifumi.shiraki.ya@hco.ntt.co.jp; kenji.ishikawa.mp@hco.ntt.co.jp; noboru.harada.pv@hco.ntt.co.jp).

Jun Muramatsu and Takehiro Moriya are with the NTT Communication Science Laboratories, Nippon Telegraph and Telephone Corporation, Soraku-gun, Kyoto-fu 619-0237, Japan (e-mail: jun.muramatsu@ntt.com; takehiro.moriya.vn@hco.ntt.co.jp).

Digital Object Identifier 10.1109/JPHOT.2022.3233092



the bit-error-rate (BER) performance of the inverse-LPS when HD-SPD and SD-SPD are used as FEC decoders. To make our simulation reflect a realistic environment, we applied the empirical parameters of the OCC experiment system from our previous work [11].

### B. LPS Architecture for the VLC System

When the LPS architecture is applied to the VLC system, a systematic FEC encoder should be placed after the DM to preserve the probabilistic shapes of the DM output sequences. With regard to turbo codes and low density parity check (LDPC) codes, polar codes were the first explicit codes proven to achieve the Shannon capacity for a binary-input discrete memoryless channel [12]. In addition, systematic polar codes (SPC) have better bit error rate (BER) performance than the original non-systematic polar codes [13]. Therefore, we applied SPC to our system in order to strengthen the systematic FEC part in the LPS architecture, which has been confirmed by Prinz et al. [14]. In addition, for outdoor applications, strong FEC codes are applied to the VLC system in order to overcome additional path loss due to long distances and potential interference from optical noise sources such as daylight and fluorescent lighting [6]. Therefore, we decided to target support of SD FEC decoders instead of HD FEC decoders as in conventional RLL-based VLC systems.

In conventional VLC systems, RLL codes keep the DC balance and maintain an equivalent ratio of 1's and 0's in the transmitted bit sequences. However, they have certain limitations, such as complex decoding, and support only HD FEC with many redundant bits in the encoded sequences. Instead of using RLL codes, our system uses the DM to keep the maximum run length of the transmitted bit stream within the flicker-free range of the system's optical clock.

Our previous work [3] introduced a run-length aware (RLA) pattern for the frozen bits of the SPC to limit the free run of 0's or 1's in the transmitted sequence. The SPC is specified by  $(z, n, \mathcal{F})$ , where  $n$  is the number of information bits encoded per codeword,  $z$  is the FEC codeword length, and  $\mathcal{F}$  is a set of  $l-n$  indices which indicate the locations of the frozen bits, where  $\mathcal{F} \subset \{1, 2, 3, \dots, l\}$ ,  $|\mathcal{F}| = z - n$ . At the designed signal-to-noise ratio (design-SNR), given an SPC with code rate  $\mathcal{R}_{\text{FEC}} = n/z$ , a construction algorithm over an additive white Gaussian noise (AWGN) channel selects the  $n$  best among  $z$  bit channels as information bit indices and the remaining  $z - n$  channels as frozen bit indices. In the original setting, all 0's are assigned to frozen bits, which increases the 0's run length of the SPC codewords. In the proposed system, our 4p-EMPDM dimmer ignores output sequences with few 0's or 1's by limiting the number of composition pairs in its codebook. In so doing, the run length of the transmitted bit stream can be kept within the flicker-free range without having to modify the polar code as in our previous work.

### C. Binary Distribution Matching

The binary DM transforms a Bernoulli  $(\frac{1}{2})$  distributed bit sequence into a nonuniform output sequence with the desired distribution. A one-to-one binary DM is an injective function

$f_{\text{DM}}$  from binary input sequences  $\mu \in \{0, 1\}^k$  to codewords  $u \in \mathcal{B}^n$ , where  $\mathcal{B}$  is the output alphabet. For binary DM,  $\mathcal{B} = \{0, 1\}$ , the function is as follows:

$$f_{\text{DM}} : \{0, 1\}^k \rightarrow \{0, 1\}^n \quad (1)$$

The binary DM outputs an  $n$ -bit sequence  $u$ , denoted as  $\bar{u}^n$ , containing a fixed number of symbols in the alphabet  $\mathcal{B} = \{0, 1\}$ . The output probability distribution  $P_A$ , which is also referred to as a type in [10], of  $\bar{u}^n$  is given as

$$P_A = (P_A(0), P_A(1)) \quad (2)$$

$$P_A(0) = \frac{n_0(u)}{n}; P_A(1) = \frac{n_1(u)}{n} \quad (3)$$

where  $n_0(u)$  and  $n_1(u)$  respectively denote the number of occurrences of 0's and 1's in the output sequence  $\bar{u}^n$ , and  $n = n_0(u) + n_1(u)$ .

*Definition 1:* Assume alphabet  $\mathcal{B} = \{0, 1\}$ , a composition of the sequence  $u$  is the ordered set of occurrences in  $u$  of each symbol from the alphabet  $\mathcal{B}$ . For binary DM, the composition  $\gamma(u)$  is defined by

$$\gamma(u) := [n_0(u), n_1(u)] \quad (4)$$

*Example 1:*  $\gamma(1011101011) = [3, 7]$ .

For constant-composition binary DM, the codebook has only the typical composition (TC)  $\gamma_m$ . The codebook of the TC is defined as

$$C_m = \{u \in \{0, 1\}^n, \gamma(u) = \gamma_m\} \quad (5)$$

The size of  $C_m$  is expressed by a multinomial coefficient as follows:

$$|C_m| = \binom{n}{\gamma_m} = \left( \frac{n!}{n_0(u)!n_1(u)!} \right) \quad (6)$$

For binary DM implemented by  $m$ -out-of- $n$  codes,  $n_1(u) = m$  and  $n_0(u) = n - m$ . The size of  $C_m$  is computed as follows:

$$|C_m| = \binom{n}{m} = \left( \frac{n!}{m!(n-m)!} \right) \quad (7)$$

*Definition 2:* The matching rate  $\mathcal{R}_{\text{DM}}$ , which indicates how many information bits are carried by each bit encoded by the binary DM, is defined as

$$\mathcal{R}_{\text{DM}} = \frac{k}{n} = \frac{\left\lfloor \log_2 \binom{n}{m} \right\rfloor}{n} \quad (8)$$

where  $\left\lfloor \log_2 \binom{n}{m} \right\rfloor$  outputs the largest  $k$  satisfying the inequality  $2^k \leq \binom{n}{m}$ .

The entropy of a discrete random variable  $A$  with alphabet  $\mathcal{B} = \{0, 1\}$  and type  $P_A$  is defined as

$$\mathbb{H}(A) = \sum_{a \in \mathcal{B}} -P_A(a) \log_2 P_A(a) \quad (9)$$

The maximum matching rate that binary DM can achieve is

$$\mathcal{R}_{\text{DM}} \leq \mathbb{H}(A) \quad (10)$$

TABLE I  
MAIN SYMBOLS AND FUNCTIONS USED IN THE PAPER

| Symbol/Function                                     | Definition  |
|---|---|
| $v, \mu, u, y$                                      | low-rate signal, input information word, DM's output sequence, FEC codeword                               |
| $v', \mu', u', y'$                                  | recovered signals at the receiver of $v, \mu, u, y$   |
| $k, z$  | length of input information word $\mu$ , and FEC codeword length  |
| $n, m$  | length of the DM's output sequence, Hamming weight of the $n$ -bit codeword                               |
| $\mathcal{B}$                                       | binary alphabet $\mathcal{B} = \{0, 1\}$  |
| $f_{\text{DM}}$                                     | fixed-length invertible mapping function that represents the DM   |
| $\mathcal{F}$                                       | set of indices which indicate locations of frozen bits  |
| $\Upsilon_0, \Upsilon_1$                            | target probability distribution of low-level and high-level dimming                                       |
| $P_A$   | output probability distribution (%) of the DM, also referred to as type $P_A$ with alphabet $\mathcal{B}$ |
| $\bar{u}^n$   | the bit sequence $u$ contains fixed $n$ symbols in the alphabet $\mathcal{B} = \{0, 1\}$                  |
| $n_0(\cdot), n_1(\cdot)$                            | number of 0's and 1's in the output sequence $\bar{u}^n$  |
| $\gamma$  | the composition which contains the number of 0's and 1's in the bit sequence $u$                          |
| $C_m,  C_m , c_m$                                   | codebook of composition $\gamma_m$ , codebook size, a codeword in the codebook $C_m$                      |
| $Z$   | the number of sequences in the codebook   |
| $\mathcal{R}_{\text{DM}}, \mathcal{R}_{\text{FEC}}$ | matching rate of the DM, FEC code rate  |
| $\mathbb{H}(\cdot), \Delta_{\text{DM}}$             | entropy and rate loss of a nonuniform sequence probabilistically shaped by the binary DM                  |
| $\Gamma(\cdot), \mathcal{A}, \mathcal{I}$           | multi-composition set, area of pixels (width $\times$ height), pixel intensity                            |
| $\delta, \epsilon$                                  | maximum run length of a sequence, number of image frames for timing synchronization                       |
| $\min(x, y), \lfloor \dots \rfloor$                 | minimum between $x$ and $y$ , floor function  |
| $\max \mathcal{A}, \min \mathcal{A}$                | the largest area and smallest area values of 50%-dimming symbols  |
| $\max \mathcal{I}, \min \mathcal{I}$                | the largest and smallest intensities of 50%-dimming symbols   |
| $\alpha, \beta, T_e$                                | fitting parameters, exposure time of the camera's image sensor  |
| $E_b, N_0, \theta$                                  | bit energy, noise density, and the ratio of the camera's exposure time and bit interval                   |
| $s, b, b_l, b_h$                                    | the gradient, center, low, and high $Y$ -intercepts of the threshold line equation                        |
| $(X_i, Y_i)$  | Coordinate of an arbitrary point  |

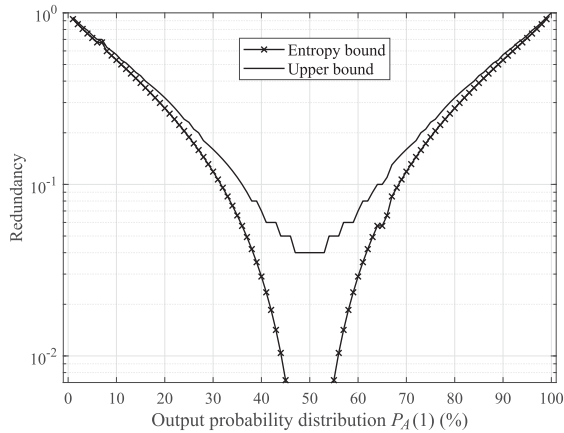


Fig. 2. Redundancy in each bit of the binary DM's output sequences, which are shaped for different output distributions. The shaped sequences have length  $n = 100$ , which is compatible with the short frame lengths in VLC specifications. The estimated redundancy is between the entropy lower bound ( $1 - \mathbb{H}(A)$ ) and the upper bound ( $1 - \mathcal{R}_{\text{DM}}$ ).

The rate loss of binary DM is formally defined as

$$\Delta_{\text{DM}} = \mathbb{H}(A) - \mathcal{R}_{\text{DM}} \quad (11)$$

Binary constant-composition distribution matching (CCDM) can be implemented by using arithmetic coding [15], [16], or subset ranking [10], to generate codewords on-the-fly. Therefore, a large codebook can be exploited without the need for storage. The CCDM output sequences are of a fixed type, which means the outputs have the same composition.

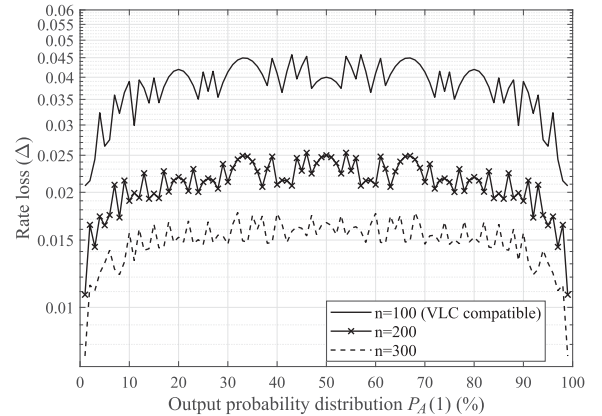


Fig. 3. Rate loss analysis of binary CCDM codewords, which are shaped for probability distributions  $0\% < P_A(1) < 100\%$ . The codewords are of different lengths  $n = 100, 200, 300$ , where  $n = 100$  is compatible with short frame specifications for VLC systems.

Fig. 2 shows the redundancy in each bit of the binary DM's shaped sequences for different output distributions. The redundancy decreases remarkably when the sequences are shaped for output distributions close to  $P_A(1) = 50\%$ . Fig. 3 shows the rate loss of nonuniform sequences probabilistically shaped by binary CCDM having different lengths  $n = 100, 200, 300$ . It can be seen that the rate loss of the binary CCDM is smaller for long codewords. Most VLC specifications, such as IEEE 802.15.7, support high-data-rate communications for infrastructure, mobile and vehicle applications [6], [17]; in particular, short VLC data frames with lengths from  $32 \sim 128$  bits are specified for physical layer specifications. Here, we evaluated a binary



DM with a block length of  $n = 100$  and FEC with a codeword length of  $l = 128$ , which are values compatible with most VLC standards.

#### D. Binary Multi-Composition Distribution Matching

Pikus et al. introduced the concept of multiple compositions for binary DM implemented with  $m$ -out-of- $n$  codes [18], where the codebook contains codewords with multiple compositions. A set of different compositions is given as

$$\Gamma = \{\gamma_1, \dots, \gamma_i\} \quad (12)$$

where  $\gamma_m = [n - m, m]$ , for  $m = 1, 2, \dots, n - 1$ . A binary multi-composition DM (MCDM) codebook is defined as

$$\mathcal{C}_{\text{MCDM}} = \{u \in \{0, 1\}^n : \gamma(u) \in \Gamma\} \quad (13)$$

Recently, a number of advanced fixed-length multi-composition probabilistic shaping techniques, such as Huffman-coded sphere shaping (HCSS) [19] and enumerative sphere shaping (ESS) [20], have been proposed. These algorithms achieve very good rate losses at short block lengths. However, HCSS and ESS are designed for an multidimensional sphere, e.g., for shaping 64-ary quadrature amplitude modulation (QAM) signals. Hence, these approaches are not suitable for our OCC system, which is mainly based on binary processing for OOK signals. Therefore, only binary DMs are considered in the evaluations described below.

One special case of multi-composition addressed by Pikus is the  $[m_L, m_U]$ -out-of- $n$  codebook, which includes codewords with a Hamming weight at least  $m_L$  and at most  $m_U$ ;  $m_L \leq n_1(u) \leq m_U$ . In our previous work, we proposed FDC, which produces codewords with type  $P_A(1)$  that can be any value in the desired probabilistic ranges [3]. The codebook of FDC can be considered equivalently to a  $[1, m]$ -out-of- $n$  codebook that contains all sequences with Hamming weights up to  $m$ , which can be expressed as  $\Gamma = \{\gamma_1, \gamma_2, \dots, \gamma_m\} = \{[n - 1, 1], [n - 2, 2], \dots, [n - m, m]\}$ .

Although the MCDM and FDC schemes achieve a lower rate loss compared with the conventional CCDDM schemes, their codebooks include shaped sequences with long free runs of 0's or 1's, which may potentially cause flicker in the VLC systems. In addition, it is challenging to implement MCDM and FDC because of their unconstrained number of compositions. This paper proposes a new shaping scheme that has a lower rate loss compared with current binary distribution matching approaches. It produces run-length-aware shaped sequences which can be applied to non-RLL VLC systems and RoI signaling applications.

### III. DIMMER BASED ON EXTENDED MULTISSET-PARTITION DISTRIBUTION MATCHING WITH FOUR COMPOSITION PAIRS (4P-EMPDM)

#### A. Binary Extended MPDM (EMPDM)

The rate loss of CCDDM increases as the block length decreases. MPDM was introduced as a way to reduce the rate loss especially for short block lengths, which is more suitable for practical implementation [18], [21]. The rate loss reduction

of MPDM results from the inclusion of CPs in addition to the TC [21] for generating non-constant-composition DMs. Pairwise partitioning is used wherein each constituent composition has a complement such that the probabilistic average of their sequences achieves the desired distribution. [21], [22] introduced a binary tree structure where each information word is split into a payload that is mapped onto a binary CCDDM sequence and a prefix that selects the composition.

*Remark 1:* Different from the conventional MPDM, where the number of sequences in a particular composition must be rounded to the nearest power of 2, we propose binary EMPDM, which extends the codebook of the conventional matching by lifting the power-of-2 constraint on each composition. To make the EMPDM implementable with a binary tree structure, we propose sharing the codebook between the TC and the first leading CP and between nearby compositions. In addition, for RoI signaling applications, we propose a 4p-EMPDM dimmer which supports two dimming levels  $\Upsilon_0$  and  $\Upsilon_1$ , where  $\Upsilon_0$  and  $\Upsilon_1$  are the typical output distributions of the dimmer for the low-rate logic-0 and logic-1, respectively.

*Definition 3:* Let  $C_m$  denote  $n$ -tuples of weight  $m$ , which form the codebook of the TC. For low-level dimming  $m = \Upsilon_0 \cdot n$ , and  $m = \Upsilon_1 \cdot n$  for high-level dimming. The number of permutations in the codebook of the CP  $\{\gamma_{m-l}, \gamma_{m+l}\}, l > 0$  can be computed as

$$Z_l = |C_{m-l}| + |C_{m+l}| = 2 \cdot \min(|C_{m-l}|, |C_{m+l}|) \quad (14)$$

The total number of permutations of the EMPDM codebook, which includes the TC and all CPs, is given as

$$Z = \sum_{l=1}^{N_{\text{pairs}}} Z_l + |C_m| = \sum_{l=1}^{N_{\text{pairs}}} (|C_{m-l}| + |C_{m+l}|) + |C_m| \quad (15)$$

where  $N_{\text{pairs}}$  denotes the number of valid CPs that fulfill the constraint  $\{\gamma_{m-l}, \gamma_{m+l}\} = 2\{\gamma_m\}, l > 0$ .

For  $\Upsilon_0 < 0.5$ ,  $\min(|C_{m-l}|, |C_{m+l}|) = |C_{m-l}|$ , from (14) and (15), we have

$$Z_{\Upsilon_0} = \sum_{l=1}^{N_{\text{pairs}}} 2 \cdot |C_{m-l}| + |C_m| = 2 \sum_{l=1}^{N_{\text{pairs}}} |C_{m-l}| + |C_m| \quad (16)$$

Similarly, for  $\Upsilon_1 > 0.5$ ,  $\min(|C_{m-l}|, |C_{m+l}|) = |C_{m+l}|$ , we have

$$Z_{\Upsilon_1} = 2 \sum_{l=1}^{N_{\text{pairs}}} |C_{m+l}| + |C_m| \quad (17)$$

The numbers of sequences in the EMPDM codebook for low-level shaping  $\Upsilon_0$  and high-level shaping  $\Upsilon_1$  are as follows:

$$\begin{aligned} Z_{\Upsilon_0} &= 2 \sum_{l=1}^{N_{\text{pairs}}} \binom{n}{\Upsilon_0 n - l} + \binom{n}{\Upsilon_0 n} \\ Z_{\Upsilon_1} &= 2 \sum_{l=1}^{N_{\text{pairs}}} \binom{n}{\Upsilon_1 n + l} + \binom{n}{\Upsilon_1 n} \end{aligned} \quad (18)$$

Because EMPDM is a fixed-length invertible mapping, the number of input bits  $k$  and the output sequence length  $n$  are fixed. Imposing the constraint  $\Upsilon_0 = 1 - \Upsilon_1$  leads to an implementation that supports two symmetric shaping levels for RoI

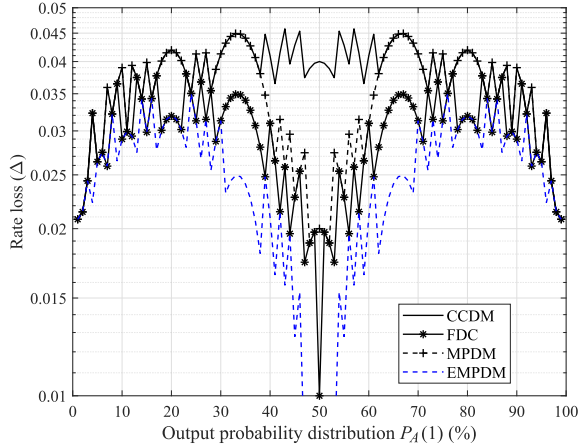


Fig. 4. Rate loss of different distribution matching schemes. The sequences are shaped for different output distributions  $1\% < P_A(1) < 99\%$ .

signaling applications. By imposing this constraint on (18), we have  $Z_{\Upsilon_0} = Z_{\Upsilon_1}$ .

*Proof:* see Appendix A.

From (8) and (18), the matching rate of EMPDM at two shaping levels can be written as

$$\mathcal{R}_{\text{EMPDM}} = \frac{\lfloor \log_2(Z_{\Upsilon_0}) \rfloor}{n} = \frac{\lfloor \log_2(Z_{\Upsilon_1}) \rfloor}{n} \quad (19)$$

The rate loss of EMPDM, denoted as  $\Delta_{\text{EMPDM}}$ , is estimated using (11) and (19). As shown in Fig. 4, it is much lower than those of other shaping methods for all output distributions. Moreover, it is symmetric with respect to  $P_A(1) = 50\%$  under the constraint  $\Upsilon_0 = 1 - \Upsilon_1$ . The symmetry properties of the matching rate and rate loss are important in designing a DM-based dimmer that enables two dimming levels at the same rate loss. Here, implementing the EMPDM by using look-up tables (LUTs) seems challenging if the EMPDM codebook has all CPs. In addition, flicker is a fundamental problem in non-RLL VLC systems, so shaped sequences with long free runs of 1's or 0's should be avoided. Therefore, in the later part of this section, we optimize the EMPDM to make it compatible with VLC-based RoI signaling applications.

### B. Proposed 4p-EMPDM Dimmer and Implementation Method

For  $1 \leq m < n$ , in order to find out how many times larger  $C_m$  is than  $C_{m-1}$ , we have

$$|C_m| / |C_{m-1}| = \binom{n}{m} / \binom{n}{m-1} = \frac{(n-m+1)}{m} \quad (20)$$

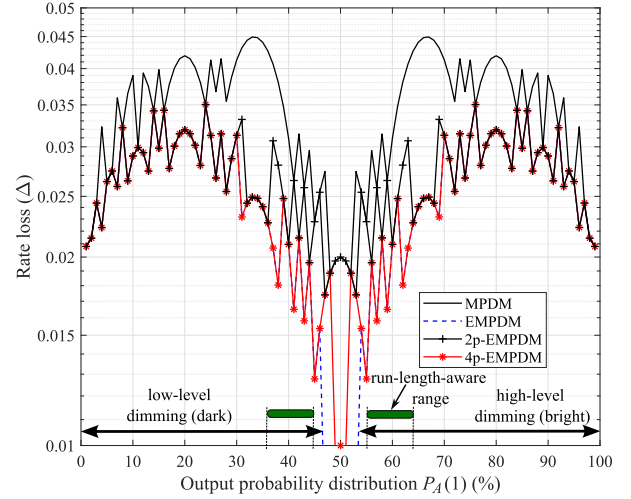


Fig. 5. Rate loss of MPDM and some instances of EMPDM when different numbers of CPs are included in the codebook of EMPDM. 4p-EMPDM is a compact version of EMPDM that produces only run-length-aware codewords for VLC applications. The arrows mark the empirical shaping ranges for the low-level dimming (logic-0) and high-level dimming (logic-1). The gap around  $P_A(1) = 50\%$  is to avoid ambiguity in detecting low-rate logic-0 and logic-1 states. The run-length-aware shaping ranges for VLC applications are marked in green.

*Example:* In the case of  $n = 100$ ,  $C_{25}$  is 452.5 times larger than  $C_{20}$  and 957293 times larger than  $C_{15}$ ; that is,  $C_{15} \ll C_{20} \ll C_{25}$ .

*Remark 2:* (20) reveals that most of the nonuniform sequences in the EMPDM codebook have TC ( $\gamma_m$ ) and leading CPs  $\{\gamma_{m-l}, \gamma_{m+l}\}$ , where  $l$  is a small positive value.

Fig. 5 shows the rate loss of the MPDM, and some instances of EMPDM when its codebook has the TC and two leading CPs (2p-EMPDM), 4 CPs (4p-EMPDM), and all CPs (EMPDM). It can be seen that the rate loss of 4p-EMPDM is equivalent to EMPDM; especially in the range  $P_A(1) < 45\%$  for low-level dimming, and the range  $P_A(1) > 55\%$  for high-level dimming. On the other hand, the rate loss of 2p-EMPDM increases due to the penalty of not including the third and fourth CPs in the codebook. For non-RLL VLC systems, codewords should have a nearly equal ratio of 1's and 0's. Therefore, lowest rate loss and DC balance are two criteria for deciding the constrained shaping ranges for the 4p-EMPDM dimmer. We conducted experimental evaluations and determined two run-length-aware shaping ranges:  $37\% < P_A(1) < 45\%$  and  $55\% < P_A(1) < 63\%$  (see Fig. 5).

Fig. 6 shows the block diagram of the proposed 4p-EMPDM dimmer, which supports two dimming levels at the same rate loss through the symmetry feature with respect to the type  $P_A(1) = 50\%$  of the rate loss, as explained in Section III-A. The dimmer includes codebooks of CPs ( $C_{m-l}, C_{m+l}$ ), where  $l = \{1, 2, 3, 4\}$ , and the codebook of TC ( $C_m$ ) and its rate loss is less than that of CCDM. Fig. 7 shows the codebook structures of the conventional MPDM, EMPDM, and 4p-EMPDM. EMPDM extends the codebook of MPDM because its composition's codebook does not have the power-of-2 constraint, as explained in Section III-A. In addition, the codebook includes only the TC



---

**Algorithm 1** Construction of the Two-Level 4p-EMPDM Dimmer and Its Binary Tree Structure.
 

---

- 1: Determine the output distributions  $\Upsilon_0, \Upsilon_1$  that produce two desired dimming levels.
  - 2: Determine the TC  $\gamma_m$  of each dimming level:  $m = \Upsilon_0.n$  for the low-level dimming and  $m = \Upsilon_1.n$  for the high-level dimming. The low-rate signal  $v$  determines the dimming level.
  - 3: Find all possible CPs that fulfill the constraint  $\{\gamma_{m-l}, \gamma_{m+l}\} = 2\{\gamma_m\}, l > 0$ .
  - 4: Remove unselected sequences in the larger of the pairs  $(C_{m-l}, C_{m+l})$ . The number of sequences after this removal is  $|C_{m-l}, C_{m+l}| = 2 \cdot \min(|C_{m-l}|, |C_{m+l}|), l = \{1, 2, 3, 4\}$ .
  - 5: Limit the main codebook to the TC and the 4 CPs  $\sum_{l=1}^{N_{\text{pairs}}=4} (C_{m-l}, C_{m+l}) + C_m$ .
  - 6: Sort the TC and the 4 CPs in descending order depending on the number of sequences in their codebooks
  - 7: Round down the total number of sequences to the nearest power of 2 ( $2^k$ ), where  $k$  is the number of input bits of the dimmer.
  - 8: Divide the dimmer's codebook into subset pairs with different lengths  $2^{k_i}$ , e.g.  $i = \{1, 2\}$  (see Fig. 8).
  - 9: Reserve  $p_l$  prefix bits to identify the subset pairs. The next bit after the prefix bits is used to identify the subset within the pair.
    - (i) For the shared typical-pairwise subsets:  $p_l = 1$
    - (ii) For the shared pairwise subsets:  $p_l = 2$
  - 10: Use  $m$ -out-of- $n$  code to map the  $k_l$ -bit payload to a shaped sequence in each subset.
- 

Fig. 9 shows the digital signal processing (DSP) flow and experimental setup of the proposed transmitter and receiver. Fig. 10 and Fig. 11 show our low-rate RoI signaling and high-rate OCC demonstration systems. Table II summarizes the settings for low-rate and high-rate experiment systems. We use a global-shutter 30-fps camera for the low-rate RoI signaling receiver that detects the dimming levels and decodes the low-rate bit stream. The Atomos Shogun 7 with attached SSDmini storage works as the video capturing and monitoring device. A VLC transmitter with a low-power LED is placed at different distances, 1.7 m, 2.9 m, and 4.2 m, from the receiver. On the other hand, we use a HS camera receiver drove at 10000 fps with exposure  $50 \mu\text{s}$ . The captured images by the HS camera are sent to a field-programmable gate array (FPGA) for processing. Beside, to evaluate performance of proposed method, we built a simulation system for the high-rate OCC system over an OCC channel.

#### A. Noise Effects and Pixel $E_b/N_0$

How noise affects image quality has been extensively studied [23], [24]. In general, noise effects differ from one imaging

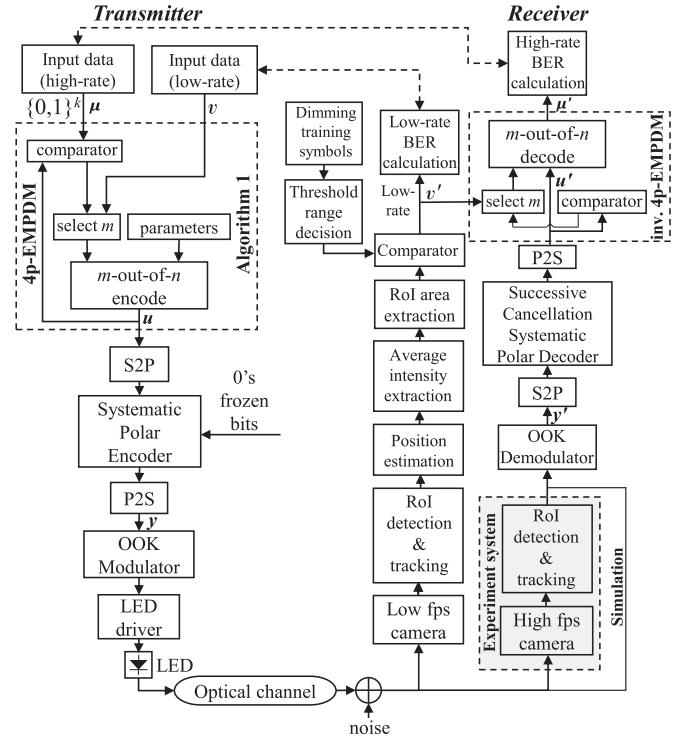


Fig. 9. DSP flow and experimental setup of the proposed transmitter and receiver.

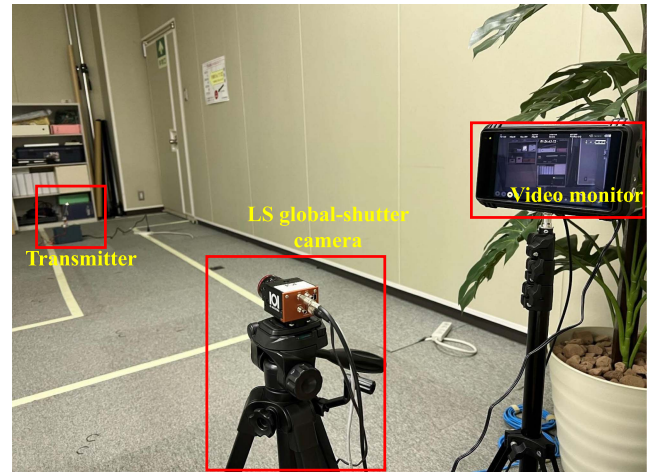


Fig. 10. Our low-rate RoI signaling demonstration system with the experiment parameters listed in Table. The visible light signals from the VLC transmitter are observed by the LS global-shutter camera. The Atomos Shogun 7 device captures the video sent from the camera and displays it on the monitor. The captured video is processed offline with MATLAB to reconstruct the transmitted messages.

system to another. For OCC systems, noise is modeled as a Gaussian distribution. The dominant noise sources are thermal noise generated by readout circuitry and shot noise due to background illumination [23]. The variance of shot noise is proportional to the area of the received pixels and the received optical intensity. The pixel noise in charge-coupled device/complementary metal-oxide semiconductor (CCD/CMOS) cameras, assuming



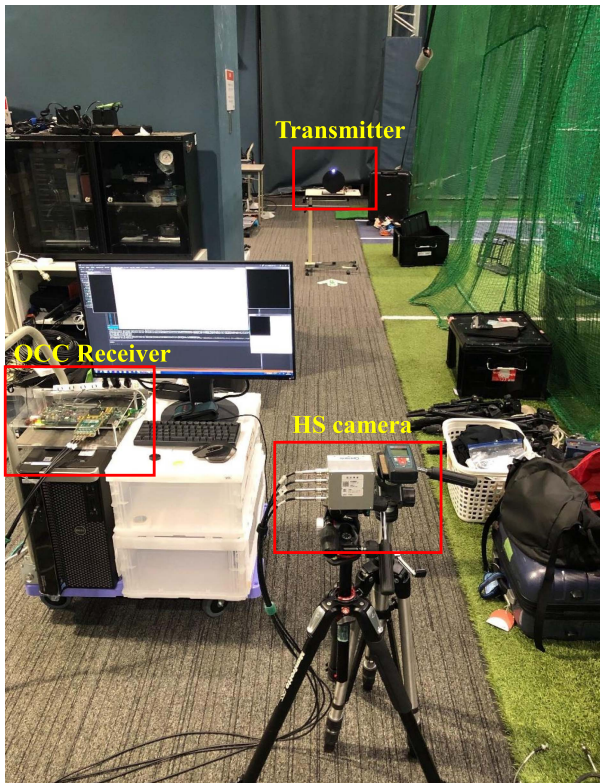


Fig. 11. Our high-rate OCC experiment system with the experiment parameters listed in Table. The signal from the LED transmitter is observed with a high-speed camera receiver. The observed signals are pre-processed by an FPGA and sent to the PC for storage.

TABLE II  
EXPERIMENTAL SETTINGS

| Parameters                      | Information/Value           |
|---------------------------------|-----------------------------|
| <i>Transmitter</i>              |                             |
| LED                             | Cree XLamp White LED XMLEZW |
| LED driver                      | 5V PWM Dimmer Controller    |
| Tx clock rate                   | 10 kHz                      |
| <i>LS-camera-based receiver</i> |                             |
| Capturing and storage           | Atomos Shogun 7             |
| Camera type                     | Victorem 2KSDI-Mini         |
| Image sensor                    | Sony Pregius IMX265         |
| Frame rate                      | 30 fps                      |
| Lens                            | LM12JC5MC                   |
| Focal length                    | 12 mm                       |
| Shutter                         | Global                      |
| Exposure time                   | 640 $\mu$ s - 6400 $\mu$ s  |
| Distances                       | 1.7 m, 2.9 m, 4.2 m         |
| <i>HS-camera-based receiver</i> |                             |
| Camera model                    | Optronis CP80-3-M-540       |
| Frame rate                      | 10000 fps                   |
| Exposure time                   | 50 $\mu$ s                  |

one bit per symbol, can be approximated as

$$\text{pixel } E_b/N_0 \approx \frac{a^2\theta}{\alpha\theta a + \beta} \quad (22)$$

where  $N_0$  is the noise density,  $E_b$  is the bit energy,  $\theta = T_e/T$  is the ratio of the camera's exposure time and the bit interval,

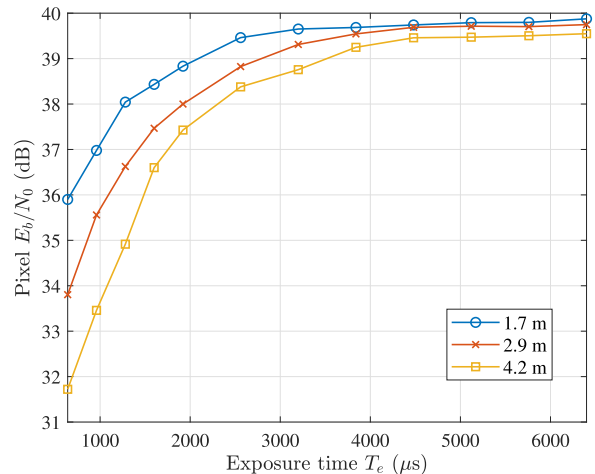


Fig. 12. Pixel  $E_b/N_0$  versus camera exposure time ( $T_e$ ) at room-scale distances of 1.7 m, 2.9 m, and 4.2 m. The results are recorded on the low-rate RoI signaling demonstration system with the experimental parameters listed in Table.

$a$  is the mark and space amplitude, and  $\alpha$  and  $\beta$  are fitting parameters. We used  $\alpha = 0.01529$  and  $\beta = 0.1973$ , which were experimentally estimated in [1], [25], to calculate the pixel  $E_b/N_0$ . Moreover, a camera with a long exposure time can be considered to be a low-pass filter attenuating high-frequency signals. Therefore, adjusting the exposure time significantly affects the pixel  $E_b/N_0$ . As shown in Fig. 12, the pixel  $E_b/N_0$  changes with the exposure time of our CMOS camera. However, when  $T_e > 4500 \mu\text{s}$ , the pixel  $E_b/N_0$  saturates at about 39.7 at distances of 1.7 m, 2.9 m, and 4.2 m. With a Tx clock rate of 20 kHz, the average brightness of one 128-bit frame requires 6.4 ms to be fully sensed by the LS camera. Therefore, we set  $T_e = 6400 \mu\text{s}$ , corresponding to a pixel  $E_b/N_0 = 39.74$ , to find the optimal shaping levels for the 4p-EMPDM dimmer.

Fig. 13 shows how noise affects the intensity and area of 50%-dimming symbols. We obtained an intensity variance of  $|\max \mathcal{I} - \min \mathcal{I}| = 14.5$  and an area variance of  $|\max \mathcal{A} - \min \mathcal{A}| = 10$ . We took the variance at the 50%-dimming level to be the within-class variance for determining the threshold range for demodulating the low-rate bit stream.

### B. Intensity-Area Thresholds

Conventional OCC systems decide the LED's ON and OFF states by making a comparison with the intensity thresholds. For determining the thresholds, our VLC transmitter sent out 100,000 symbols shaped by the 4p-EMPDM dimmer at  $30\% < P_A(1) < 70\%$ . Fig. 14 shows the received symbols that were shaped by the dimmer at  $\Upsilon_0 = 30\%$  for logic-0 and  $\Upsilon_1 = 70\%$  for logic-1. It can be seen that there is no difference in the pixel intensities of the symbols shaped by the dimmer at  $\Upsilon_1 = 70\%$ ; the receiver can detect only the differences in the pixels area of the symbols shaped with different compositions. On the other hand, the intensity variance is considerable with symbols shaped by the dimmer at  $\Upsilon_0 = 30\%$ . The reason is that the pixel intensity reaches saturation when the dimming level is close to 70%,

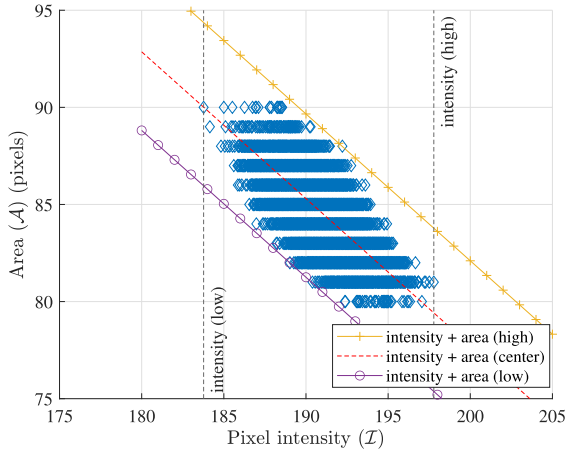


Fig. 13. Noise affecting both intensity and area of received pixels: within-class variance of 10700 symbols transmitted at dimming level of 50% captured by the LS global-shutter camera. The variance between low and high intensity is to ensure the shaping gap around  $P_A(1) = 50\%$ , wherein the dimmer avoids producing bit sequences with  $P_A(1)$  in this gap. The receiver is placed 4.2 m from the VLC transmitter.

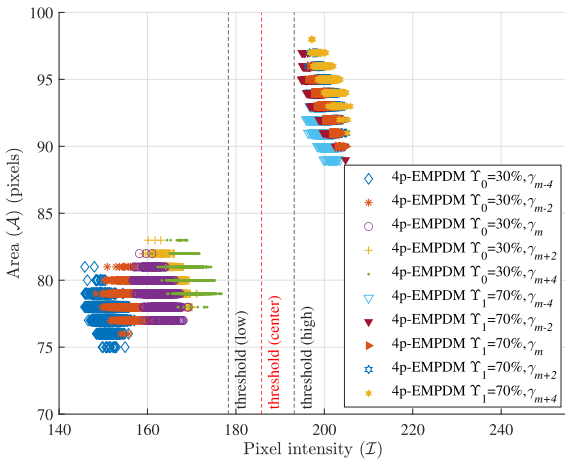


Fig. 14. Two-class classification using intensity thresholds. The camera captures two dimming levels in which symbols are shaped by the 4p-EMPDM dimmer with ratios  $\Upsilon_0 = 30\%$  for logic-0, and  $\Upsilon_1 = 70\%$  for logic-1. Only intensity information is used to determine the thresholds for the logic-0/logic-1 decision. The camera sensor's exposure time is  $T_e = 6400 \mu\text{s}$ . The camera-based receiver is placed 4.2 m from the VLC transmitter.

where the VPPM was confirmed to show the best performance at this dimming level [1]. This finding reveals that the pixels' area of the received signal is useful for demodulating the data in addition to the pixel intensity. Therefore, our LS-camera-based receiver uses the intensity and area information of the captured signals for demodulating data and determining thresholds.

Specifically, the low, center, and high thresholds are used for determining the threshold range, which is the range between the low and high thresholds. The within-class variances caused by the noise effects determine the width of the range, as explained in Section IV-A. Threshold range is defined to avoid ambiguity in detecting nearby dimming levels. The equation of the center

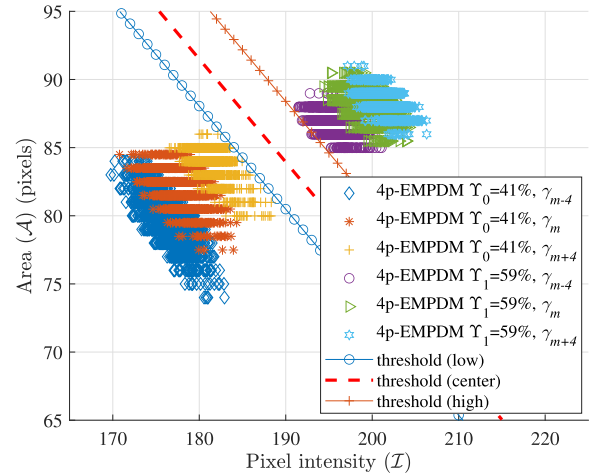


Fig. 15. Two-class classification using intensity-area thresholds. The camera captures dimming symbols shaped by the 4p-EMPDM dimmer at typical shaping ratios  $\Upsilon_0 = 41\%$  for logic-0 and  $\Upsilon_1 = 59\%$  for logic-1. Both the intensity and area of the captured pixels are used to determine the intensity-area thresholds. The exposure time of the camera sensor is  $T_e = 6400 \mu\text{s}$ . The camera-based receiver is placed 4.2 m from the VLC transmitter.

threshold is

$$Y = s.X + b \quad (23)$$

where  $s$  and  $b$  denote the gradient and the  $y$  intercept of the threshold line respectively, which can be computed using the following formulas:

$$s = \frac{\min \mathcal{A} - \max \mathcal{A}}{\max \mathcal{I} - \min \mathcal{I}} \quad (24)$$

$$b = Y - s.X = \max \mathcal{A} - s.\min \mathcal{I} \quad (25)$$

where  $\mathcal{A}$  and  $\mathcal{I}$  denote the area (width  $\times$  height) and average intensity of the captured pixels, respectively. The high and low threshold lines can be determined using straight line equations  $Y = s.X + b_h$  and  $Y = s.X + b_l$ , where  $b_h$  and  $b_l$  are determined by replacing the coordinates of the farthest points above and below the center threshold in equation (23). To check if an arbitrary point  $(X_i, Y_i)$  is above or below the center threshold, the point's coordinate  $(X_i, Y_i)$  should be inserted into the threshold line equation (23); then  $Y_i$  should be compared with  $s.X_i + b$ . If  $Y_i < s.X_i + b$ , the point is below the line; otherwise if  $Y_i > s.X_i + b$ , the point is above the threshold.

Fig. 15 shows the received symbols shaped by the 4p-EMPDM dimmer at  $\Upsilon_0 = 41\%$  and  $\Upsilon_1 = 59\%$ . When using the intensity-area thresholds, the typical shaping levels move closer to 50%; specifically, from 30% to 41% for logic-0 and from 70% to 59% for logic-1. As a result, the rate loss of the dimmer decreases from 0.031 to 0.0165 (see Fig. 5), which means that the matching rate increases with the proposed area-intensity thresholds.

## V. RESULTS AND DISCUSSION

Performance comparison of binary distribution matching schemes is experimental evaluated by rate loss (see Fig. 4 and

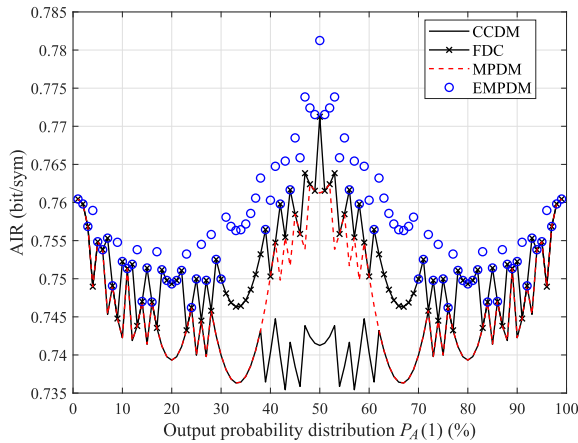


Fig. 16. AIR analysis of binary distribution matching schemes at different output probability distributions which produce different dimming ratios.

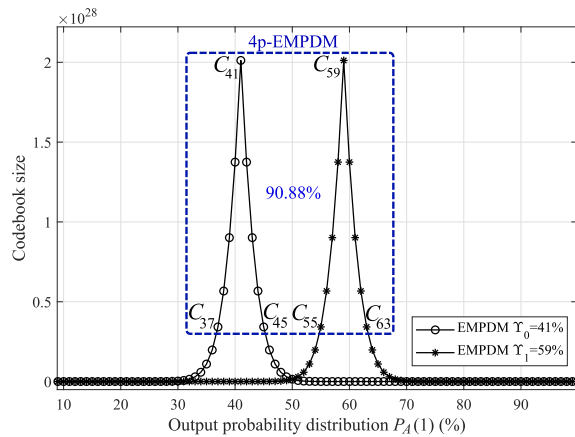


Fig. 17. Number of sequences in the codebooks of the EMPDM and 4p-EMPDM dimmers. The blue dashed line is for the codebook of the 4p-EMPDM dimmer. The solid line is for the codebook of the EMPDM dimmer with all CPs. The results of the experimental optimization with intensity-area thresholds (see Fig. 15) give  $\Upsilon_0 = 41\%$  and  $\Upsilon_1 = 59\%$  as the optimal empirical output distributions of the 4p-EMPDM dimmer for low-rate logic-0 and logic-1, respectively.

Fig. 5), and achievable information rate (AIR) [10], [21]. We evaluate the AIR of binary DMs at different output probability distributions. Our numerical AIR evaluation method is presented in Appendix B. Fig. 16 shows the AIR performances of binary DMs. It can be seen that at shaping ratios  $\Upsilon_0 = 41\%$  and  $\Upsilon_1 = 59\%$ , AIR improvement of EMPDM is 0.02, 0.01 and 0.01 compared with CCDM, FDC and MPDM, respectively.

Fig. 17 shows the codebook sizes of the 4p-EMPDM and EMPDM dimmers at  $\Upsilon_0 = 41\%$  and  $\Upsilon_1 = 59\%$ . These optimal output distributions were experimentally determined when the intensity-area thresholds were used to decide low-rate logic levels. It can be seen that the codebook size of the 4p-EMPDM dimmer is 90.88% that of the EMPDM dimmer due to most of the quantity belonging to the TC and the 4 CPs. In the ranges  $P_A(1) = [37\%, 45\%]$  and  $P_A(1) = [55\%, 63\%]$ , the rate loss of the 4p-EMPDM dimmer is equivalent to that of the EMPDM dimmer (see Fig. 5). As explained in Section III-B,

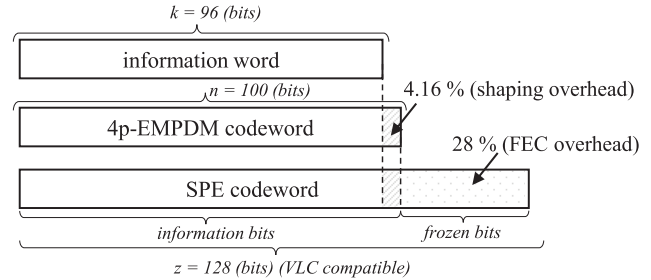


Fig. 18. Overheads of 4p-EMPDM dimmer at  $\Upsilon_0 = 41\%$  and  $\Upsilon_1 = 59\%$ , and FEC encoding (SPE).

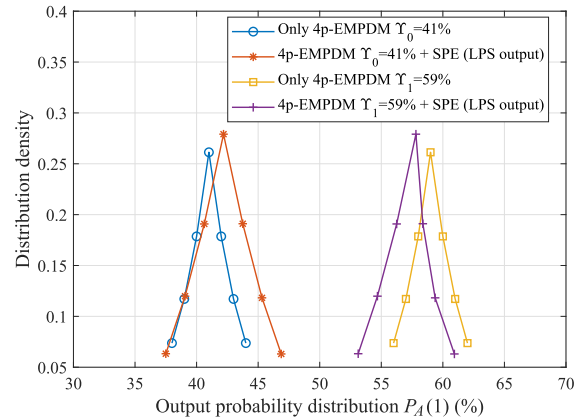


Fig. 19. Distribution density of the output sequences produced by the 4p-EMPDM dimmer at optimal output distributions  $\Upsilon_0 = 41\%$  and  $\Upsilon_1 = 59\%$ . The results were recorded at the outputs of the 4p-EMPDM dimmer and the SPE (LPS output).

the 4p-EMPDM dimmer only produces sequences with roughly equal ratios of 0's and 1's. Hence, compared with other binary distribution matching approaches, the 4p-EMPDM is suitable for non-RLL VLC systems because the run length of its output sequence is constrained for flicker mitigation.

The Fig. 18 shows the overheads of 4p-EMPDM dimmer and FEC encoding. Coding overhead is the ratio of the numbers of redundant bits and information bits, which can be expressed as a percentage. Overhead of 4p-EMPDM is 4.16%, and SPE (FEC) overhead is 28%.

The proposed 4p-EMPDM and inverse 4p-EMPDM dimmer can be easily implemented using simple arithmetic and logic operations recursively. We referred to encoding and decoding flows of  $m$ -out-of- $n$  code for implementing 4p-EMPDM and inverse 4p-EMPDM dimmer [16]. The complexity estimation of the proposed method is presented in Table IV.

Although the systematic FEC encoder better preserves the output probability distribution of the 4p-EMPDM dimmer compared with the non-systematic FEC encoders, the logical operations on the generator and parity matrixes of the systematic FEC encoder usually change the output distribution of the dimmer's codewords. Therefore, we examined the output distributions of the LPS's output sequences in a Monte Carlo simulation. Fig. 19 depicts the output probability distributions of 100,000 information words shaped by the 4p-EMPDM dimmer and encoded by



TABLE III  
COMPARISON WITH HYBRID MODULATION SCHEMES IN IEEE P802.15.7 M (TG7M) PHY-IV MODES [2]

| RoI signaling technique       | RLL   | Optical clock rate | FEC   | Bit rate               | Spectral efficiency (single LED) |
|-------------------------------|---|--------------------|---|------------------------|----------------------------------|
| Twinkle VPPM                  | N/A   | 16 kHz             | Reed-Solomon (15,11)                                | 4 kbps                 | 0.25 (bits/s)/Hz                 |
| HS-PSK                        | code rate 1/2 for S2-PSK;<br>None for DS8-PSK | 10 kHz             | Temporal error-correction;<br>Outer FEC with GF(16) | 1.38 kbps*             | 0.138 (bits/s)/Hz <sup>†</sup>   |
| FDC                           | None  | 12.6 kHz           | SPC (128,100)                                       | 8.95 kbps              | 0.71 (bits/s)/Hz                 |
| 4p-EMPDM dimmer<br>(Proposed) | None  | 6 kHz - 12.6 kHz   | SPC (128,100)                                       | 9.45 kbps <sup>‡</sup> | 0.75 (bits/s)/Hz                 |

\* Bit rate = 22 kbps (16 LEDs). <sup>†</sup> Two light sources, 8 LEDs for each source, spectral efficiency (single LED) = bit rate/(clock rate $\times$ 8 $\times$ 2).

<sup>‡</sup> Theoretical bit rate of the high-rate bit stream at optical clock rate of 12.6 kHz.

TABLE IV  
COMPLEXITY ESTIMATION OF THE PROPOSED METHOD

|                          | 4p-EMPDM | Inv. 4p-EMPDM |
|--------------------------|----------|---------------|
| Addition, Subtraction    | 8        | 17            |
| Multiplication, Division | 2        | 4             |
| Modulus arithmetic (Mod) | 0        | 1             |
| Comparison               | 5        | 10            |

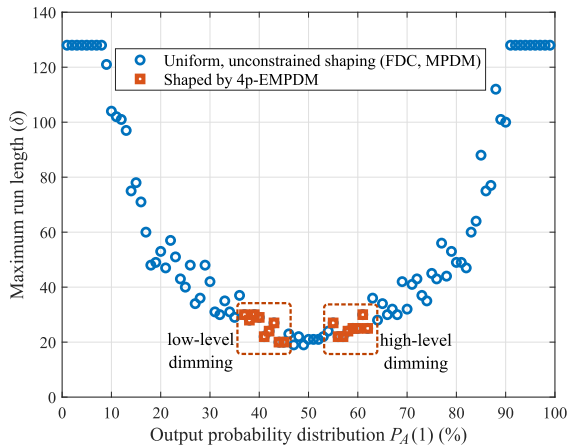


Fig. 20. Maximum run-length analysis of bit sequences at the output of the LPS. The bit sequences are shaped for different output distributions from 1% to 99%. The dashed squares show the ranges of the maximum run length when the bit sequences are shaped by the 4p-EMPDM dimmer at  $\Upsilon_0 = 41\%$  and  $\Upsilon_1 = 59\%$ . Due to the unconstrained number of CPs, FDC and MPDM produce output sequences with long run lengths.

the SPE following the LPS architecture. It can be seen that the SPE makes the output distributions of the dimmer move slightly closer to the  $P_A(1) = 50\%$ . For RoI signaling applications, the low-rate logic levels is made from the two dimming levels; therefore, the output distributions of the LPS symbols corresponding to the two dimming levels must not overlap in order for them to be discriminated by the LS-camera-based receiver.

We also evaluated the maximum run length of the bit sequences at the LPS output, denoted as  $\delta$ . As shown in Fig. 20, when 128-bit sequences are shaped by the 4p-EMPDM dimmer at  $\Upsilon_0 = 41\%$  and  $\Upsilon_1 = 59\%$ ,  $\delta = 30$ ; this compares with  $\delta = 126$  for uniform and unconstrained shaping. For flicker mitigation, the LED's brightness changes within the maximum flickering time period (MFTP  $\leq 5$  ms) [6]. Hence, with  $\delta =$

30, our system guarantees flicker-free operation at optical clock rates higher than 6 kHz without using an RLL code.

Table III compares the proposed method with related works on the image-sensor communication PHY-IV modes added to TG7m [2]. The minimum clock rate of our system is 6 kHz, which is smaller than that of the reference RoI signaling systems. Bearing in mind that FEC codes with code rates  $\mathcal{R}_{\text{FEC}} \in (0.5, 0.8)$  have been proposed in the PHY II modes of IEEE 802.15.7 and the PHY-IV modes of TG7m [1], [6], we decided to evaluate our system with a systematic polar code (128,100) with  $\mathcal{R}_{\text{FEC}} = 0.78$ ; the reason for selecting the short frame length  $l = 128$  is explained in Section II-C. Our system achieved a spectral efficiency of 0.75 (bits/s)/Hz with the proposed 4p-EMPDM dimmer. Here, the dimmer shaped the symbols at  $\Upsilon_0 = 41\%$  and  $\Upsilon_1 = 59\%$  with a matching rate  $\mathcal{R}_{4\text{p-EMPDM}} = 0.96$  and rate loss  $\Delta_{4\text{p-EMPDM}} = 0.0165$ . The spectral efficiency of our system was thus much better than those of the reference systems based on hybrid modulation schemes. For a fair comparison, we considered the single-LED VLC transmitter as a baseline. The proposed system surpassed the related work in terms of the minimum clock rate, bit rate, and spectral efficiency.

Furthermore, the CDR issues should be considered in our non-RLL OCC system. Let  $\epsilon$  denote the number of image frames required by the HS camera to synchronize the timing and decode the bit sequence on the receiver. Our previous work experimentally confirmed that when there is a clock difference between the transmitter and receiver, the bit error rate (BER) performance is stable when  $\epsilon \leq 100$  [11]. Fig. 20 shows that a bit sequence transmitted with our system has a maximum run length of  $\delta = 30$ . By referring to  $\delta$ , to guarantee the CDR in case a long run of 1's or 0's appears in the bit sequence, we decided to set  $\delta \leq \epsilon \leq 100$ .

In fact, the two camera-based receivers use different mechanisms for demodulating the received light signals. The HS-camera-based receiver decodes the high-rate bit stream by detecting LED's ON-OFF states, whereas the LS-camera-based receiver detects two dimming levels of the LED to decode logic-0 and logic-1 states. Therefore, we evaluated the error probability of the low-rate stream on the RoI signaling demonstration system with the experimental settings listed in Table II. In addition, we performed numerical simulations in an AWGN channel for the high-rate stream to examine the performance of the inverse 4p-EMPDM dimmer and effectiveness of the SD-SPD in the proposed system.



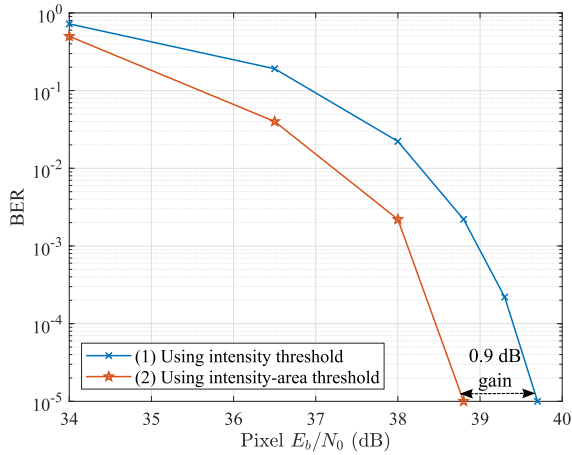


Fig. 21. BER versus pixel  $E_b/N_0$  of the low-rate stream that was practically evaluated on the low-rate RoI signaling demonstration system. The pre-determined thresholds are used to differentiate logic states from dimming levels. There are two scenarios in which the thresholds are determined: (1) when only the pixel intensity information of the training symbols is used; (2) when both the area and intensity information of the training symbols are involved.

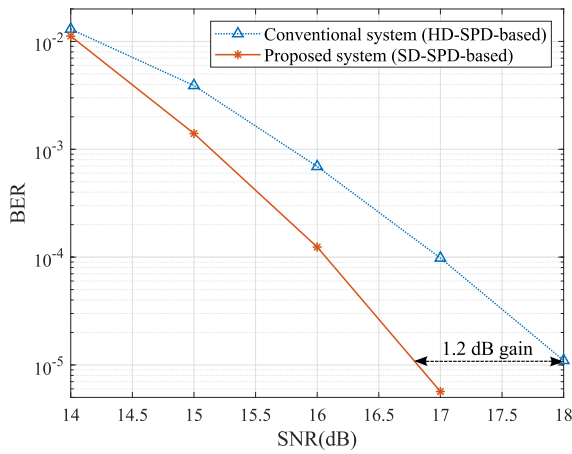


Fig. 22. BER performances of simulated high-rate streams in OCC channel. In the proposed system, the SD-SPC decodes the bit stream before the inverse 4p-EMPDM dimmer recovers the original messages. BER performance of the conventional system based on HD-SPC is shown for reference.

Fig. 21 shows the BER performance versus pixel  $E_b/N_0$  of the low-rate bit stream. The results were recorded when the 4p-EMPDM dimmer operated at  $\Upsilon_0 = 41\%$  and  $\Upsilon_1 = 59\%$ . The BER of the low-rate stream was measured in terms of the misdetection probability between the two dimming levels. Specifically, the LS-camera-based receiver compared the pixels area and intensity of the received signals with a pre-determined threshold range to demodulate the bit values. Both the intensity and the intensity-area thresholds were involved in the evaluation. As a result, the system achieved a 0.9 dB performance gain at a BER =  $1E-5$  when using the intensity-area thresholds. The BER performance of the low-rate stream is depicted in Fig. 21; it was estimated without the support of any error-correction code.

Another critical performance metric is the so-called BER, which is the received BER after FEC decoding. Fig. 22 presents

the BER performances of the high-rate bit streams in conventional system and proposed system. In the proposed system, the bit stream was decoded by the SD-SPD thanks for the non-RLL feature. On the other hand, the bit stream was decoded by the HD-SPD in the conventional system due to limitations of the SISO RLL decoder. Fig. 22 shows that the coding gain achieved with the proposed system and the conventional systems differ by 1.2 dB at a BER =  $1E-5$ . In summary, because of the non-RLL feature, the proposed system can use the SD FEC decoders to improve its reliability.

## VI. CONCLUSION

This paper introduced a two-level dimmer based on binary distribution matching for visible light RoI signaling applications. Our dimmer controls the dimming by switching the output probability distribution of the high-rate bit sequence depending on the value of the low-rate signal. We proposed the EMPDM, which extends the codebook of the conventional MPDM by sharing codewords between nearby compositions. A new binary tree structure was introduced for the implementation of the EMPDM. The proposed EMPDM achieves a lower rate loss than those of the MPDM, FDC, and CCDM shaping schemes because of its extended codebook. To make EMPDM compatible with VLC-based RoI signaling applications, we introduced the 4p-EMPDM, limiting the EMPDM's codebook to TC and 4 CPs. The proposed 4p-EMPDM dimmer produces only run-length-aware codewords for non-RLL VLC systems. In addition, we optimized the shaping levels of the 4p-EMPDM dimmer using the threshold range, where both intensity and area information of the received training symbols are exploited. Experimental results revealed that the proposed system achieves excellent spectral efficiency compared with systems based on hybrid modulation techniques such as twinkle VPPM or HS-PSK. In addition, the 4p-EMPDM dimmer reduces the maximum run length of the LPS output sequences by 4.27 times. Hence, flicker mitigation is guaranteed for any optical clock rate higher than 6 kHz, even without an RLL code. Moreover, because of the non-RLL feature, the proposed system can use the SD FEC decoding to improve its reliability.

## APPENDIX A

### PROOF OF $Z_{\Upsilon_0} = Z_{\Upsilon_1}$

The following derivations prove the numbers of sequences in the EMPDM codebook for low-level shaping  $\Upsilon_0$  and high-level shaping  $\Upsilon_1$  are equivalent.

Assume  $\Upsilon_0 = 1 - \Upsilon_1$ , where  $\Upsilon_0 \in (0\%, 50\%)$ ,  $\Upsilon_1 \in (50\%, 100\%)$ . We have

$$\begin{aligned} \binom{n}{\Upsilon_1 n} &= \binom{n}{(1 - \Upsilon_0)n} = \binom{n}{n - \Upsilon_0 n} \\ &= \frac{n!}{(\Upsilon_0 n)!(n - \Upsilon_0 n)!} = \binom{n}{\Upsilon_0 n} \end{aligned} \quad (26)$$

Similarly, for  $l \in \{1, 2, \dots, N_{\text{pairs}}\}$ , we have

$$\begin{aligned} \binom{n}{\Upsilon_1 n + l} &= \binom{n}{(1 - \Upsilon_0) n + l} \\ &= \binom{n}{n - \Upsilon_0 n + l} = \frac{n!}{(\Upsilon_0 n - l)! (n - \Upsilon_0 n + l)!} \\ &= \frac{n!}{(\Upsilon_0 n - l)! (n - (\Upsilon_0 n - l))!} = \binom{n}{\Upsilon_0 n - l} \end{aligned} \quad (27)$$

From (18)(26)(27), we have

$$\begin{aligned} Z_{\Upsilon_1} &= 2 \sum_{l=1}^{N_{\text{pairs}}} \binom{n}{\Upsilon_1 n + l} + \binom{n}{\Upsilon_1 n} \\ &= 2 \sum_{l=1}^{N_{\text{pairs}}} \binom{n}{\Upsilon_0 n - l} + \binom{n}{\Upsilon_0 n} = Z_{\Upsilon_0} \end{aligned} \quad (28)$$

## APPENDIX B

### AIR EVALUATION FOR A BINARY DM

The numerical achievable information rate (AIR) for finite-length binary DMs, referred to as  $\text{AIR}_{\text{DM}}$ , is given by

$$\text{AIR}_{\text{DM}} = \mathcal{R}_{\text{BMD}} - \Delta_{\text{DM}} \quad (29)$$

where  $\mathcal{R}_{\text{BMD}}$  denotes the bit-metric decoding (BMD) rate as defined in [9]. In case of PAS with capacity-achieving codes, we have

$$\mathcal{R}_{\text{BMD}} \equiv I_{\text{PAS}} \quad (30)$$

where  $I_{\text{PAS}}$  is the information content per OOK symbol in bits per symbol, which is given as  $I_{\text{PAS}} = \mathcal{R}_{\text{FEC}}$ .

For the numerical AIR of a binary DM, (29) is simplified as follow

$$\text{AIR}_{\text{DM}} = \mathcal{R}_{\text{FEC}} - \Delta_{\text{DM}} \quad (31)$$

## ACKNOWLEDGMENT

The authors would like to thank the anonymous reviewers for their comments which greatly helped to improve the presented paper.

## REFERENCES

- [1] M. D. Thieu, T. L. Pham, T. Nguyen, and Y. M. Jang, "Optical-RoI-signaling for vehicular communications," *IEEE Access*, vol. 7, pp. 69873–69891, 2019.
- [2] T. Nguyen, A. Islam, T. Yamazato, and Y. M. Jang, "Technical issues on IEEE 802.15.7 m image sensor communication standardization," *IEEE Commun. Mag.*, vol. 56, no. 2, pp. 213–218, Feb. 2018.
- [3] D.-P. Nguyen, Y. Shiraki, J. Muramatsu, and T. Moriya, "A probabilistic shaping approach for optical region-of-interest signaling," *IEEE Photon. Technol. Lett.*, vol. 34, no. 6, pp. 309–312, Mar. 2022.
- [4] H. Wang and S. Kim, "Dimming control systems with polar codes in visible light communication," *IEEE Photon. Technol. Lett.*, vol. 29, no. 19, pp. 1651–1654, Oct. 2017.
- [5] J. Noh, S. Lee, J. Kim, M. Ju, and Y. Park, "A dimming controllable VPPM-based VLC system and its implementation," *Opt. Commun.*, vol. 343, pp. 34–37, 2015.
- [6] S. Rajagopal, R. D. Roberts, and S.-K. Lim, "IEEE 802.15.7 visible light communication: Modulation schemes and dimming support," *IEEE Commun. Mag.*, vol. 50, no. 3, pp. 72–82, Mar. 2012.
- [7] H. Wang and S. Kim, "Soft-input soft-output run-length limited decoding for visible light communication," *IEEE Photon. Technol. Lett.*, vol. 28, no. 3, pp. 225–228, Feb. 2016.
- [8] G. Böcherer, P. Schulte, and F. Steiner, "Probabilistic shaping and forward error correction for fiber-optic communication systems," *J. Lightw. Technol.*, vol. 37, no. 2, pp. 230–244, Jan. 2019.
- [9] G. Böcherer, F. Steiner, and P. Schulte, "Bandwidth efficient and rate-matched low-density parity-check coded modulation," *IEEE Trans. Commun.*, vol. 63, no. 12, pp. 4651–4665, Dec. 2015.
- [10] T. Fehenberger, D. S. Millar, T. Koike-Akino, K. Kojima, and K. Parsons, "Parallel-amplitude architecture and subset ranking for fast distribution matching," *IEEE Trans. Commun.*, vol. 68, no. 4, pp. 1981–1990, Apr. 2020.
- [11] Y. Shiraki et al., "A demodulation method using a Gaussian mixture model for unsynchronous optical camera communication with on-off keying," *J. Lightw. Technol.*, vol. 39, no. 6, pp. 1742–1755, Mar. 2021.
- [12] E. Arikan, "Channel polarization: A method for constructing capacity-achieving codes for symmetric binary-input memoryless channels," *IEEE Trans. Inf. Theory*, vol. 55, no. 7, pp. 3051–3073, Jul. 2009.
- [13] E. Arikan, "Systematic polar coding," *IEEE Commun. Lett.*, vol. 15, no. 8, pp. 860–862, Aug. 2011.
- [14] T. Prinz et al., "Polar coded probabilistic amplitude shaping for short packets," in *Proc. IEEE 18th Int. Workshop Signal Process. Adv. Wireless Commun.*, 2017, pp. 1–5.
- [15] P. Schulte and G. Böcherer, "Constant composition distribution matching," *IEEE Trans. Inf. Theory*, vol. 62, no. 1, pp. 430–434, Jan. 2016.
- [16] T. V. Ramabadran, "A coding scheme for m-out-of-n codes," *IEEE Trans. Commun.*, vol. 38, no. 8, pp. 1156–1163, Aug. 1990.
- [17] A.-M. Cailean and M. Dimian, "Impact of IEEE 802.15.7 standard on visible light communications usage in automotive applications," *IEEE Commun. Mag.*, vol. 55, no. 4, pp. 169–175, Apr. 2017.
- [18] M. Pikus and W. Xu, "Arithmetic coding based multi-composition codes for bit-level distribution matching," in *Proc. IEEE Wireless Commun. Netw. Conf.*, 2019, pp. 1–6.
- [19] T. Fehenberger, D. S. Millar, T. Koike-Akino, K. Kojima, K. Parsons, and H. Griesser, "Huffman-coded sphere shaping and distribution matching algorithms via lookup tables," *J. Lightw. Technol.*, vol. 38, no. 10, pp. 2826–2834, May 2020.
- [20] Y. C. Gültekin, W. J. van Houtum, A. G. Koppelaar, F. M. J. Willems, and W. J. van Houtum, "Enumerative sphere shaping for wireless communications with short packets," *IEEE Trans. Wireless Commun.*, vol. 19, no. 2, pp. 1098–1112, Feb. 2019.
- [21] T. Fehenberger, D. S. Millar, T. Koike-Akino, K. Kojima, and K. Parsons, "Multiset-partition distribution matching," *IEEE Trans. Commun.*, vol. 67, no. 3, pp. 1885–1893, Mar. 2019.
- [22] D. S. Millar, T. Fehenberger, T. Koike-Akino, K. Kojima, and K. Parsons, "Distribution matching for high spectral efficiency optical communication with multiset partitions," *J. Lightw. Technol.*, vol. 37, no. 2, pp. 517–523, Jan. 2019.
- [23] S. Hranilovic and F. R. Kschischang, "A pixelated MIMO wireless optical communication system," *IEEE J. Sel. Topics Quantum Electron.*, vol. 12, no. 4, pp. 859–874, Jul./Aug. 2006.
- [24] N. Saeed, S. Guo, K.-H. Park, T. Y. Al-Naffouri, and M.-S. Alouini, "Optical camera communications: Survey, use cases, challenges, and future trends," *Phys. Commun.*, vol. 37, 2019, Art. no. 100900.
- [25] R. D. Roberts, "IEEE 802.15.7r1 - Intel OCC Proposal," IEEE Standards Assoc., Jan. 2016. [Online]. Available: <https://bit.ly/3dUL7ZK>
- [26] T. Yoshida, M. Karlsson, and E. Agrell, "Performance metrics for systems with soft-decision FEC and probabilistic shaping," *IEEE Photon. Technol. Lett.*, vol. 29, no. 23, pp. 2111–2114, Dec. 2017.